Materials Performance and Characterization

doi:10.1520/MPC20190206 / Vol. 9 / No. 5 / 2020 / available online at www.astm.org

Matthias Merzkirch[1] and Tim Foecke[2]

Investigation of the Interlaminar Shear Properties of Fiber-Reinforced Polymers via Flexural Testing Using Digital Image Correlation

Reference

M. Merzkirch and T. Foecke, "Investigation of the Interlaminar Shear Properties of Fiber-Reinforced Polymers via Flexural Testing Using Digital Image Correlation," *Materials Performance and Characterization* 9, no. 5 (2020): 666–674. https://doi.org/10.1520/MPC20190206

ABSTRACT

The determination of the interlaminar properties of laminate composites to date has included a few direct measurement techniques: the standardized short-beam test via three-point flexural testing and the double beam shear test via five-point flexural testing. These test methods are limited to a determination of the apparent interlaminar strength, whereas the full stress–strain behavior cannot be determined. The double beam shear test allows for a calculation of the shear modulus, provided that four additional elastic, in-plane properties have been determined in advance via three additional types of tests. The present work includes a comparison of the three-point short-beam test, the nonstandardized four-point flexural test, and the double beam shear test (requiring small span-length-to-thickness ratios for the shear loading to become dominant). The tests are carried out on unidirectional carbon fiber–reinforced composite (CFRP-UD) with a symmetric layup. The experiments are accompanied by photomechanical investigations using digital image correlation (DIC) to visualize the phenomenology of shear deformation. The novelty of this approach includes the use of the DIC-determined shear strains, which show a parabolic distribution across the specimen's thickness. The DIC-calculated maximum shear strain across the thickness is used for a full description of the stress–strain behavior with a focus on the elastic loading range to evaluate the shear modulus. Interlaminar shear strengths and shear moduli determined from all three types of tests are compared with the intralaminar shear properties.

Keywords

fiber-reinforced composite (FRP), digital image correlation (DIC), unidirectional reinforcement, unidirectional (UD), carbon fiber, carbon fiber–reinforced composite (CFRP), shear modulus, shear strength, intralaminar

Manuscript received August 9, 2019; accepted for publication December 2, 2019; published online July 10, 2020. Issue published October 15, 2020.

[1] Guest Researcher, National Institute of Standards and Technology (NIST), NIST Center for Automotive Lightweighting (NCAL), 100 Bureau Dr., Gaithersburg, MD 20899, USA (Corresponding author), e-mail: matthias.merzkirch@nist.gov, https://orcid.org/0000-0001-6463-9493

[2] National Institute of Standards and Technology (NIST), NIST Center for Automotive Lightweighting (NCAL), 100 Bureau Dr., Gaithersburg, MD 20899, USA

Introduction

The reliable investigation of the mechanical behavior of composite materials under different loading conditions (types of loading, loading rates, and environmental conditions) is of great interest to those modeling the deformation and damage behavior of structural components used in automotive and aerospace engineering. The brittle nature of carbon fiber–reinforced polymer (CFRP) composites poses a challenge in testing those materials. The determination of the in-plane and through-thickness shear properties (strength, strain, and moduli) of flat laminate sheet materials is of great interest, and many different testing procedures have been developed within the last decades to attempt to generate the needed data.

According to some studies,[1–4] more than ten different testing methods exist to determine the interlaminar (through-thickness) and intralaminar (in-plane) shear properties, including the modulus and strength[4] of unidirectionally (UD) reinforced composite laminates. For the determination of the interlaminar shear properties of UD-reinforced composite sheet material, standardized compressive testing[5] of a notched specimen is limited to only strength values, whereas the standardized V-notched beam test (also known as the "Iosipescu" test)[6] can be used for very thick sheet materials.

The standardized short-beam test via three-point (3pt) flexural loading[7,8] is commonly used for the determination of the apparent[7] interlaminar shear strength. However, a determination of the strains and therefore shear moduli from the full stress–strain response cannot be made. For flexural testing of small span-length-to-thickness ratios (L/h), shear loading becomes dominant. Based on the shear stress distribution for 3pt and four-point (4pt) bending across the thickness (in y-direction), with fibers oriented in x-direction, the through-thickness shear stress is as follows:

$$\tau_{xy}(y) = \tau_{yx}(y) = \frac{3 \cdot F}{w \cdot h^3} \cdot \left(\frac{h^2}{4} - y^2\right) \tag{1}$$

The maximum is at the centerline of the specimen ($y = 0$, neutral axis) and is used to determine the interlaminar shear strength[7,8]:

$$\tau_{\max} = \frac{3 \cdot F}{4 \cdot w \cdot h} \tag{2}$$

using the force F and the width w of the specimen.

The double beam shear test via five-point (5pt) flexural testing, ISO 19927:2018, *Fibre-Reinforced Plastic Composites—Determination of Interlaminar Strength and Modulus by Double Beam Shear Test*,[9] allows for a determination of the maximum shear stress at the midplane for a balanced fiber–reinforced polymer according to:

$$\tau_{\max} = \frac{33 \cdot F}{64 \cdot w \cdot h} \tag{3}$$

The advantage of the double beam shear test is the possibility of calculating the interlaminar shear modulus by measuring the deflection V in the high shear zones, where the positive root of the following equation indicates the interlaminar shear modulus G_{31}, as indicated by ISO 19927:2018[9]:

$$G_{31} = \frac{C_2 \cdot \left(1 - \frac{43}{s} \cdot C_1\right)}{16 \cdot C_1 \cdot \left(1 - \frac{25}{8 \cdot s} \cdot C_1\right)} \cdot \left(-1 \pm \sqrt{1 + \frac{128 \cdot C_1 \cdot \left(1 - \frac{25}{8 \cdot s} \cdot C_1\right)}{s \cdot \left(1 - \frac{43}{s} \cdot C_1\right)^2}}\right) \tag{4}$$

With s being the compliance (V/F) from the elastic part of the force–displacement curve, and the constant:

$$C_1 = \frac{L^3}{12,288 \cdot \sum_{i=1}^{n}(E_i \cdot I_i)} \tag{5}$$

With a term considering the inverse of the bending stiffness matrix D:

$$\sum_{i=1}^{n}(E_i \cdot I_i) = \frac{w}{D_{11}^{-1}} \tag{6}$$

The geometric constant:

$$C_2 = \frac{L}{128 \cdot k \cdot w \cdot h} \tag{7}$$

includes the shear correction factor k (=5/6, according to ISO 19927:2018,[9] as a universal approach).

By using classical lamination theory, the calculation of the interlaminar shear modulus G_{31} requires four additional elastic, in-plane properties, including the Young's moduli (E_L, E_T); Poisson's ratio (υ_{LT}) and the in-plane shear modulus (G_{21}), which have to be determined via three additional types of tests. The longitudinal (L) and transverse (T) moduli and Poisson's ratio are usually determined via tensile tests. The in-plane shear modulus can be determined via V-notched specimen testing[6] or by 10° off-axis tensile testing.[10]

Applying digital image correlation (DIC) allows for the easy full-field mapping of the deformations (in-plane and out-of-plane for stereo DIC) and strains (normal and shear), revealing the pattern of deformation and damage throughout the specimen. As early as 2000, the use of DIC for the visualization of shear zones in a 4-mm-thick CFRP specimen (loaded via 3pt short-beam testing and using a single 0.5-megapixel [MP] camera) was already successfully shown.[11]

The current work describes the use of DIC for full-field strain and deformation response while flexural testing of unidirectionally carbon fiber–reinforced (CFRP-UD) rectangular specimens with a nominal reinforcing volume fraction of 50 %.

Experimental

MATERIALS

The prototypical material investigated in this work was a unidirectional carbon fiber (with a nonround cross-sectional geometry and an average diameter of 6.9 µm) reinforced (nonstitched) composite made from epoxy prepregs. Nominally 12 prepreg layers were stacked up to a thickness of the cured balanced laminate sheet material of about 2.4 mm, with a reported reinforcing volume fraction of 50 %, resulting in an average thickness of 200 µm per ply. **Figure 1*A*** depicts a representative cross section of the plaque. The wavy nature of the single layers as well as pores (black spots) can be seen.

Table 1 summarizes the average quasistatic elastic tensile results of the composite in longitudinal (L) and transverse (T) directions. The degree of orthotropicity (E_L/E_T) is about 15 (6 %), representing a high anisotropy. The in-plane shear modulus has been determined via 10° off-axis tensile testing[10] to be $G = 4.23$ GPa with a standard deviation of ±0.06 GPa.

TESTING DETAILS

The unidirectional carbon fiber–reinforced composite is loaded in symmetric 3pt, 4pt (distance loading rollers one-half of the support span L), and 5pt (with 3 support rollers at the bottom, see **fig. 2**) bending with a diameter of the rollers of 6.35 mm (see further geometric details in **Table 2** and **fig. 1*B***).

The displacement-controlled tests have been conducted on an electromechanical testing machine at a nominal rate of 1 mm/min. The specimen's side face was prepared for DIC measurement with commercially available

FIG. 1

(*A*) Representative cross section: thickness along vertical *y*-direction and (*B*) specimens for 3pt, 4pt, and 5pt testing.

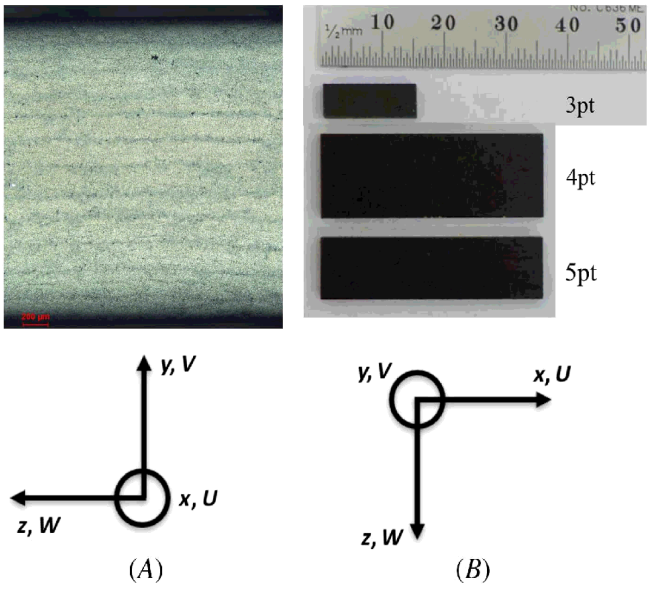

TABLE 1

Quasistatic (0.0001 s^{-1}) elastic properties from uniaxial tensile testing of UD in longitudinal and transverse directions (taken from investigations followed from Powell et al.[14])

	E, GPa	ν
0° (L)	124.6 ± 0.8	0.33 ± 0.04
90° (T)	8.1 ± 0.3	0.023 ± 0.010

FIG. 2

Field-of-view of left camera from 5pt bending setup with speckled specimen.

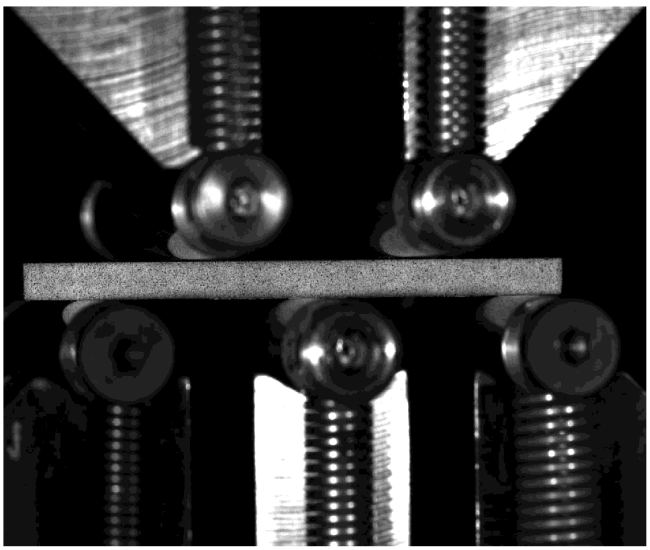

matte white spray paint, which has been applied directly onto the specimen. After drying, matte black spray paint has been applied directly onto the specimen by airbrush to create a random speckle pattern. For stereo-DIC measurement, two 9.1 MP (3,376 by 2,704 px) cameras (with a stereo angle of approximately 15° to 17° and

TABLE 2
Geometries of the waterjet cut specimens and details about testing setup

	3pt	4pt	5pt
Specimen width w in mm	5 ($\approx 2 \times h$ in ASTM D2344/D2344M-16[8])	13	9.6 ($< 5 \times h$ in ISO 19927:2018[9])
Specimen length l in mm	15 ($\approx 6 \times h$ in ASTM D2344/D2344M-16[8])	36	35.9 ($\approx 15 \times h$ in ISO 19927:2018[9])
Support span L in mm	12.3 ($> 4 \times h$ in ASTM D2344/D2344M-16[8])	30	28.3 ($> 10 \times h$ in ISO 19927:2018[9])

Note: ASTM D2344/D2344M-16, *Standard Test Method for Short-Beam Strength of Polymer Matrix Composite Materials and Their Laminates*.

a standoff distance of approximately 420 mm) and 105-mm fixed focal length lenses have been used. For data acquisition and analysis, a commercially available DIC software package has been used. The image acquisition rate was set to 2 Hz. The image scale was approximately 13 µm per pixel, and the DIC pattern size was approximately 3 px to 6 px, measured via the line intersection method. For data analysis, the chosen subset size was 19 px to 21 px and the step size was 7 px to 10 px to maximize the spatial resolution. This conforms with *A Good Practices Guide for Digital Image Correlation*,[12] which states that the subset size should be at least three times the average speckle size and the step size a third to a half the subset size. For further analysis, the following coordinate system has been adopted: the abscissa is parallel to the specimen axis, and the ordinate shows along the thickness of the specimen, in loading direction (compare also **fig. 1**). Engineering strain has been calculated using the DIC software package using a smoothing filter size of 15 data points. Further details about the DIC setup will be published by Merzkirch.[13]

Results and Discussion

MECHANICAL RESPONSE

Figure 3 shows the vertical deformation of specimens loaded in 3pt, 4pt, and 5pt bending as contour plots in the (undeformed) reference coordinates. For 3pt and 4pt bending, the maximum absolute deflection V*, located at the midpoint between the support rollers, has been used. For 5pt bending, the deflection V* between loading roller and middle support roller where fracture occurred has been used.

FIG. 3

DIC-calculated deflection V contour plots at $\tau_{max}/2$ in reference coordinates for (*A*) 3pt, (*B*) 4pt, and (*C*) 5pt.

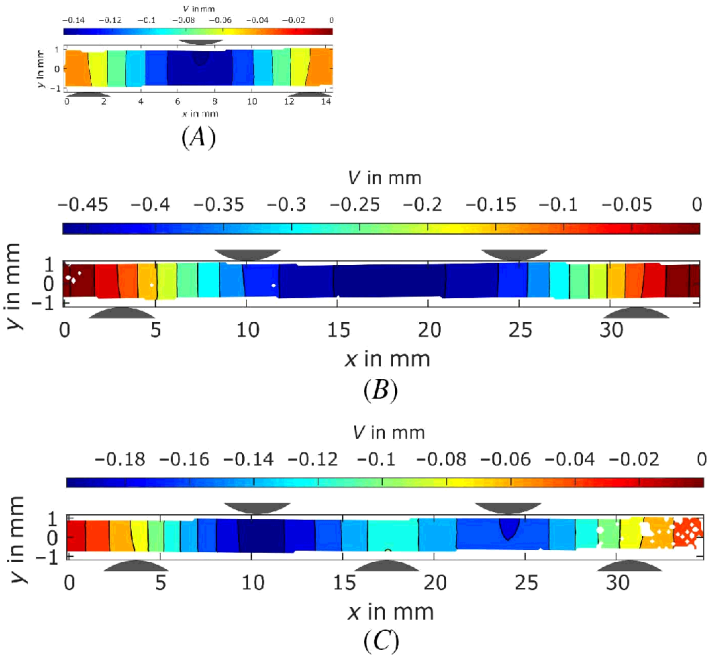

Figure 4A shows the experimental shear stress–deflection curves, with indications of the onset of delamination. Because of the different loading conditions and specimen widths, the compliances differ, with the highest compliance (smallest slope) for the 4pt test. All curves show a nonlinear region, with the smallest for the 5pt test. Delamination occurred after reaching the maximum shear stress for all types of tests, just after start of the force drop. Deviations due to specimen geometry inhomogeneities may affect the onset of delamination.

Figure 5 depicts postmortem fractographic investigations of the 3pt and 4pt specimens across the width focusing only on the shear-related failures. Because the 5pt specimen did not fully delaminate along the length, only the specimen's side face enclosing the region of the interlaminar damage is shown, where delamination can hardly be seen on the right side. Both 3pt and 4pt specimens show an asymmetric delamination, with the crack location deviating from the midplane where the interlaminar planes below and above the midplane, respectively, have delaminated.

Figure 4B visualizes a potential bias in determining the interlaminar shear strength using the normalized version of equation (1) for the symmetrical shear stress distribution across the thickness with idealized (straight) 12 layers. The deviation from the maximum shear stress (apparent interlaminar shear strength) at the midplane is given in percent for each layer. Because of the parabolic character of the shear stress evolution, the interlaminar shear strength of the first layer(s) beside the midplane is only 2.8 % smaller than the maximum shear strength. Delamination between layer 2 and 3 off the midplane leads to strength that is 11.1 % smaller.

Figure 6 depicts the shear strain γ_{xy} distribution as contour plots for all types of tests, at comparable scales. Both the 3pt and 4pt specimen show extrema left and right from the loading roller(s) with a zone of reduced shear

FIG. 4 (*A*) Maximum shear stress–deflection curves (*B*) normalized theoretical shear stress distribution across the normalized specimen thickness with 12 layers (dashed lines).

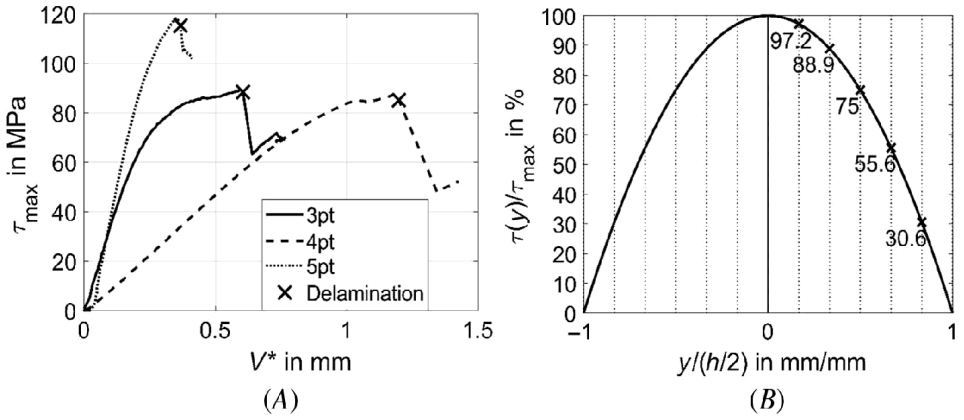

FIG. 5 Fractography of specimens for (*A*) 3pt, (*B*) 4pt (speckle side is on the left), and (*C*) for 5pt.

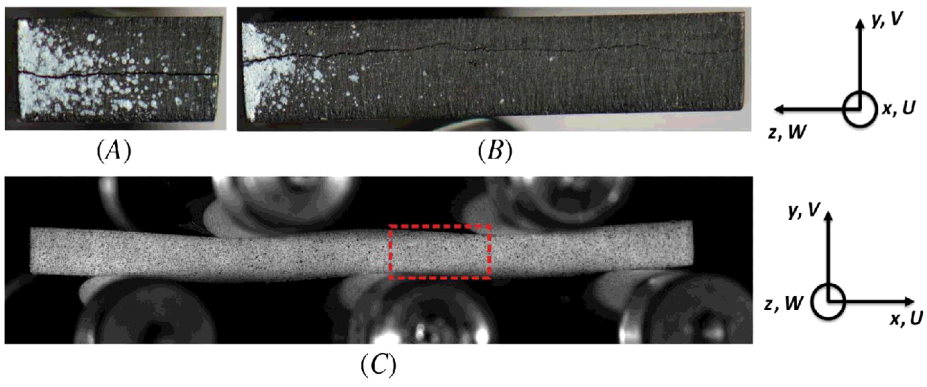

FIG. 6

DIC-calculated shear strain γ_{xy} distribution in the specimen's reference coordinate system (x–y) as contour plots at $\tau_{max}/2$ for (*A*) 3pt, (*B*) 4pt, and (*C*) 5pt.

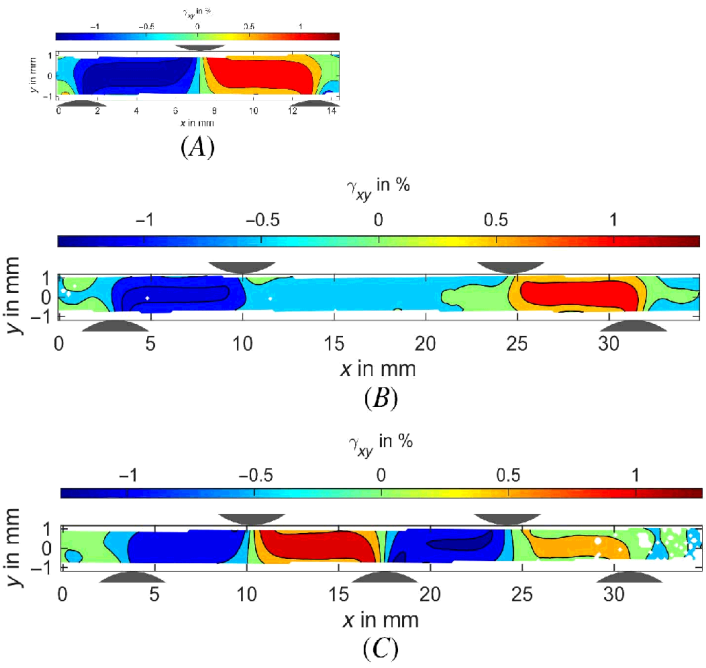

in the middle for the 4pt specimen. The 5pt specimen shows alternating shear strains along the specimen's length with the highest (absolute) shear strains in the middle part of the beam. The 3pt and 5pt specimens show more pronounced roller-induced shear bands.

QUANTITATIVE PHOTOMECHANICAL INVESTIGATION

A more detailed investigation of the shear strains across the thickness of the 3pt loaded beam is shown in figure 7*A*. Selected shear strain line plots (taken at 3/4 L, $x \approx 11$ mm, see fig. 6*A*) across the thickness emphasize the parabolic distribution with the maximum (absolute) value in the middle (note that $y = 0$ does not coincide with the specimen's centerline). Using the shear strain extrema over the whole test duration, the evolution of the shear stress–shear strain, depicted in figure 7*B* can be plotted for different locations (1/4 L, $x \approx 4$ mm, see fig. 6*A* and 3/4 L) with indication of delamination being on the right side (at 3/4 L).

FIG. 7 (*A*) 3pt beam shear strain γ_{xy} distributions across the thickness at 3/4 L, for selected points between $\tau = 10$ MPa to $\tau_{max}/2$. (*B*) Resulting maximum shear stress–maximum shear strain curves at 1/4 L ("Left") and 3/4 L ("Right").

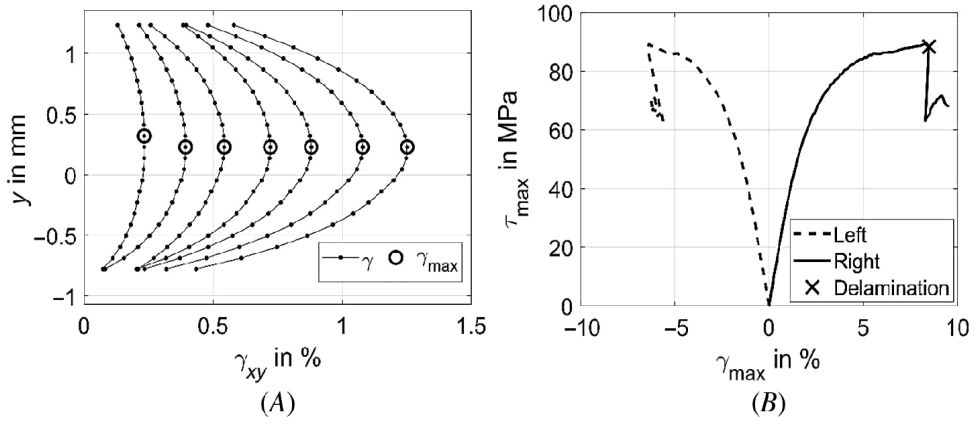

FIG. 8 (*A*) Distribution of the shear moduli along the specimen's length for 3pt. (*B*) Comparison of inter- and intralaminar shear moduli and shear strengths (average values and standard deviation from 2 tests per testing configuration, 10° off-axis results from Merzkirch and Foecke[10]).

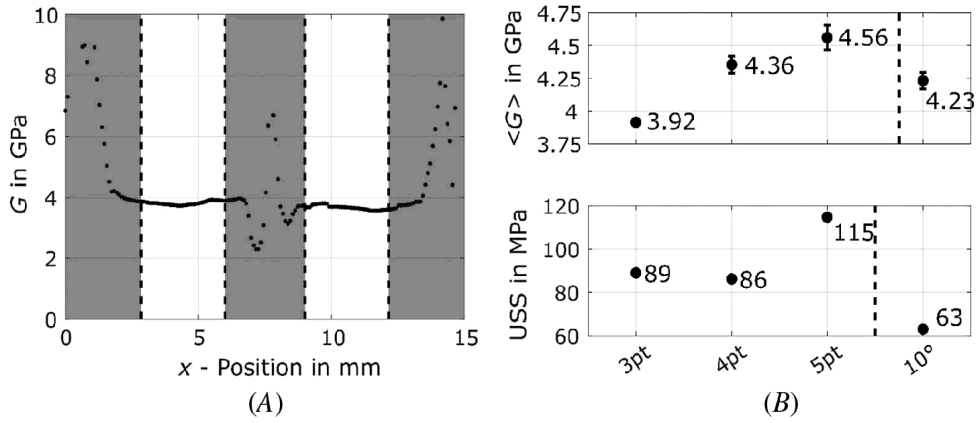

The procedure described is implemented in a self-written code and expanded along the whole length of the beam. For a further investigation of the shear modulus, shear strain values between 0.2 % to 0.6 % (based on ASTM D5379/D5379M-12, *Standard Test Method for Shear Properties of Composite Materials by the V-Notched Beam Method*[6]) are investigated. Using that range, shear moduli along the whole specimen length can be calculated (see **fig. 8*A***). High fluctuations result from strain perturbations near the support rollers on the left and right, as well as from the loading roller in the middle of the beam.

Conclusions

This contribution is a comparative study of different interlaminar (and intralaminar) shear testing methods for transversely isotropic materials, showing the benefit of using DIC as noncontact measurement for standardized flexural testing. The 3pt, 4pt, and 5pt short-beam tests have been compared in terms of interlaminar shear properties such as modulus and strength. The novelty is the application of DIC for measuring and calculating displacements and shear strains that are used to determine the shear modulus. A self-written code has been used to extract the shear strain extrema across the thickness of the specimen and over the whole loading range to evaluate a full stress–strain response and the shear moduli along the specimen's length. The results show huge fluctuations near the loading and support rollers due to strain perturbations and a relatively homogeneous distribution of the shear moduli at a distance from these locations.

By focusing on the values of the shear moduli between the rollers (nonshaded area in **fig. 8*A***), the resulting shear moduli for 3pt and 4pt can be extracted and compared with the calculated shear modulus from 5pt bending (based on the four predefined elastic properties from Merzkirch and Foecke[10]; see **fig. 8*B*** top) having the highest value. The maximum shear strength (ultimate shear strength [USS], see **fig. 8*B*** bottom) is reached via 5pt testing, which is approximately 30 % higher than the values determined via 3pt and 4pt, which are both comparable in spite of different specimen geometries. Because of the transversely isotropic character of unidirectionally reinforced fiber composites, a comparison between inter- and intralaminar shear properties can be made and is given in **figure 8*B***. With the intralaminar shear modulus being close to the average shear modulus from flexural testing, the intralaminar shear strength is minimum in comparison to all flexural tests. In summary, the shear properties from 5pt bending show the highest values. Future investigation should clarify if the alternating shear strain along the specimen's length (see **fig. 6*C***) or more contact leads to a higher constraint and therefore to a higher shear strength and modulus.

A more detailed sensitivity analysis and a comparison to V-notched specimens will be given by Merzkirch,[13] in which also a detailed investigation of other occurring strains while performing flexural testing will be provided.

ACKNOWLEDGMENTS

M. Merzkirch is sponsored by the NIST Guest Researcher program. The authors thank E. Pompa (NIST) for waterjet cutting, C. Amigo (NIST) for manufacturing the flexural fixtures, and L. A. Powell for uniaxial tensile testing results.

References

1. D. Purslow, *The Shear Properties of Unidirectional Carbon Fibre Reinforced Plastics and Their Experimental Determination, Current Paper ARC-CP-1381* (London: Aeronautical Research Council, 1977).
2. S. Lee and M. Munro, "Evaluation of In-Plane Shear Test Methods for Advanced Composite Materials by the Decision Analysis Technique," *Composites* 17, no. 1 (January 1986): 13–22. https://doi.org/10.1016/0010-4361(86)90729-9
3. S. Chaterjee, D. Adams, and D. W. Oplinger, *Test Methods for Composites: A Status Report—Volume III: Shear Test Methods, Report No. DOT/FAA/CT-93/17, III* (Washington, DC: United States Department of Transportation, 1993).
4. J. Summerscales, "Shear Modulus Testing of Composites," in *Composite Structures 4, Volume 2: Damage Assessment and Material Evaluation*, ed. I. H. Marshall (Dordrecht, the Netherlands: Springer Nature, 1987), 305–316.
5. *Standard Test Method for In-Plane Shear Strength of Reinforced Plastics*, ASTM D3846-08 (2015) (West Conshohocken, PA: ASTM International, approved September 1, 2015). https://doi.org/10.1520/D3846-08R15
6. *Standard Test Method for Shear Properties of Composite Materials by the V-Notched Beam Method* (Superseded), ASTM D5379/D5379M-12 (West Conshohocken, PA: ASTM International, approved July 15, 2012). https://doi.org/10.1520/D5379_D5379M-12
7. *Fibre Reinforced Plastic Composites–Determination of Apparent Interlaminar Shear Strength by Short Beam-Method*, DIN EN ISO 14130:1998-02 (Berlin: Deutsches Institut für Normung, 1998).
8. *Standard Test Method for Short-Beam Strength of Polymer Matrix Composite Materials and Their Laminates*, ASTM D2344/D2344M-16 (West Conshohocken, PA: ASTM International, approved July 1, 2016). https://doi.org/10.1520/D2344_D2344M-16
9. *Fibre-Reinforced Plastic Composites—Determination of Interlaminar Strength and Modulus by Double Beam Shear Test*, ISO 19927:2018 (Geneva, Switzerland: International Organization for Standardization, 2018).
10. M. Merzkirch and T. Foecke, "10° Off-Axis Tensile Testing of Carbon Fiber Reinforced Polymers Using Digital Image Correlation," in *Mechanics of Composite and Multi-functional Materials, Volume 5*, ed. R. Singh and G. Slipher (Cham, Switzerland: Springer Nature, 2020), 55–62.
11. L. G. Melin, J. M. Neumeister, K. B. Pettersson, H. Johansson, and L. E. Asp, "Evaluation of Four Composite Shear Test Methods by Digital Speckle Strain Mapping and Fractographic Analysis," *Journal of Composites, Technology and Research* 22, no. 3 (July 2000): 161–172. https://doi.org/10.1520/CTR10636J
12. International Digital Image Correlation Society, *A Good Practices Guide for Digital Image Correlation*, ed. E. M. C. Jones and M. A. Iadicola (International Digital Image Correlation Society, 2018).
13. M. Merzkirch, *Mechanical Characterization Using Digital Image Correlation: Advanced Fibrous Composite Laminates* (Cham, Switzerland: Springer Nature) (forthcoming).
14. L. A. Powell, W. E. Leucke, M. Merzkirch, K. Avery, and T. Foecke, "High Strain Rate Mechanical Characterization of Carbon Fiber Reinforced Polymer Composites Using Digital Image Correlations," *SAE International Journal of Materials and Manufacturing* 10, no. 2 (2017): 138–146. https://doi.org/10.4271/2017-01-0230